Vitreous carbon micro-lattice structures

Alan J. Jacobsen[1,*], Sky Mahoney[1], William B. Carter[1], Steven Nutt[2]

1. HRL Laboratories, Sensors and Materials Laboratory, 3011 Malibu Canyon Rd., Malibu, CA 90265, USA
2. University of Southern California, Department of Chemical Engineering and Materials Science, 3651 Watt Way, VHE 602, Los Angeles, CA 90089-0241, USA

Abstract: A new approach is presented to fabricate open-cellular carbon materials with an ordered, lattice-type micro-scale architecture. The carbon micro-lattice materials were fabricated by pyrolyzing a polymer precursor template formed from an interconnected three-dimensional array of self-propagating photopolymer waveguides. Impregnating the polymer precursor template with acrylonitrile increased the carbon yield of the material from 19% to 46%. Structural analysis and density measurements of the solid carbon phase are consistent with vitreous carbon. Compression experiments yielded a compressive modulus (E) of 1.1 GPa and a failure strength (σ_f) of 10.2 MPa for a structure with relative density of 12.8%.

*Corresponding author: ajjacobsen@hrl.com

1. Introduction

Porous vitreous carbon materials have applications as catalyst supports, filters, heat transfer media, and high-surface-area electrodes for electrochemical devices [1], [2], [3], [4], [5], [6] and [7]. These applications benefit from the distinct physical properties of solid vitreous carbon, such as low permeability to gases, high strength, electrical conductivity, relatively high oxidation resistance, and chemical inertness [8] and [9].

Alan J. Jacobsen, Sky Mahoney, William B. Carter, Steven Nutt, Vitreous carbon micro-lattice structures, Carbon, Volume 49, Issue 3, March 2011, Pages 1025-1032, ISSN 0008-6223, http://dx.doi.org/10.1016/j.carbon.2010.10.059.

In general, most approaches for creating porous vitreous carbon materials are stochastic in nature, which result in irregular cell shapes and size distributions. Some methods involve foaming an adequate polymer precursor system [10] or casting a polymer precursor around a sacrificial template such as NaCl [11]. Subsequent pyrolysis of the polymer precursors result in open-cell vitreous carbon foams with average pore diameters ranging from 35 to over 300 μm depending on the exact parameters of the process used.

The most common method for generating open-cellular vitreous carbon materials involves the use of a reticulated polyurethane foam template [1] and [3]. In this method, an open-cellular polymer foam is infiltrated and swelled by a high-carbon-yield monomer (generally polyfurfuryl alcohol or a phenolic resin). Excess monomer is removed from the open porosity of the reticulated foam, and subsequent heat treatments first polymerize the monomer and then carbonize the material. Aside from volume reduction during pyrolysis, the resulting open-cellular carbon foam features pore sizes and shapes modeled directly from the precursor polyurethane foam. The final product is generally termed reticulated vitreous carbon (RVC) [3].

In this work, we demonstrate the formation of ordered open-cell vitreous carbon structures using a periodic, ordered open-cell micro-lattice polymer precursor material recently developed in our lab [12]. The micro-lattice precursor structure is formed by an interconnected three-dimensional array of self-propagating photopolymer waveguides. The polymer micro-lattice formation process affords significant flexibility in the range of unit cell feature sizes, relative density, and resulting micro-scale architecture [13] and [14]. The RVC template approach is highly compatible with our precursor micro-lattice material, in particular the ability to capture the unit cell architecture of the open-cellular polymer structure. As with the fabrication of RVC foams, the open-cellular polymer

Alan J. Jacobsen, Sky Mahoney, William B. Carter, Steven Nutt, Vitreous carbon micro-lattice structures, Carbon, Volume 49, Issue 3, March 2011, Pages 1025-1032, ISSN 0008-6223, http://dx.doi.org/10.1016/j.carbon.2010.10.059.

precursor structures are swollen with a high-carbon-yielding monomer to reduce the volumetric shrinkage and mass loss during pyrolysis. However, unlike the phenolic-based resins that polymerize by a relatively slow step-growth condensation reaction [15], we use acrylonitrile as the high-carbon-yield monomer, which can be polymerized by a rapid free radical polymerization when exposed to UV light [16]. The carbon micro-lattice structures were subjected to compression loading to demonstrate the deformation behavior of the lattice architecture under mechanical loading and the results are compared to the compression behavior of RVC foams.

2. Experimental

2.1 Polymer micro-lattice precursor preparation

Polymer micro-lattice samples were fabricated from an interconnected pattern of self-propagating photopolymer waveguides [12]. Briefly, the process involves exposing a mask with a square pattern of circular apertures placed over a liquid thiol-ene monomer system. The mask is exposed simultaneously to four collimated beams generated from a mercury arc lamp. Each collimated beam has a 40° equal incident angle off the mask surface but is rotated 90° about the mask normal, resulting in the octahedral-type repeating unit cell shown in Fig. 1. The resulting strut (or truss member) diameter d was approximately 200 μm, and the node-to-node spacing L was 1.4 mm for all samples fabricated for this study. Further details regarding the polymer micro-lattice fabrication process can be found elsewhere [13] and [14].

Alan J. Jacobsen, Sky Mahoney, William B. Carter, Steven Nutt, Vitreous carbon micro-lattice structures, Carbon, Volume 49, Issue 3, March 2011, Pages 1025-1032, ISSN 0008-6223, http://dx.doi.org/10.1016/j.carbon.2010.10.059.

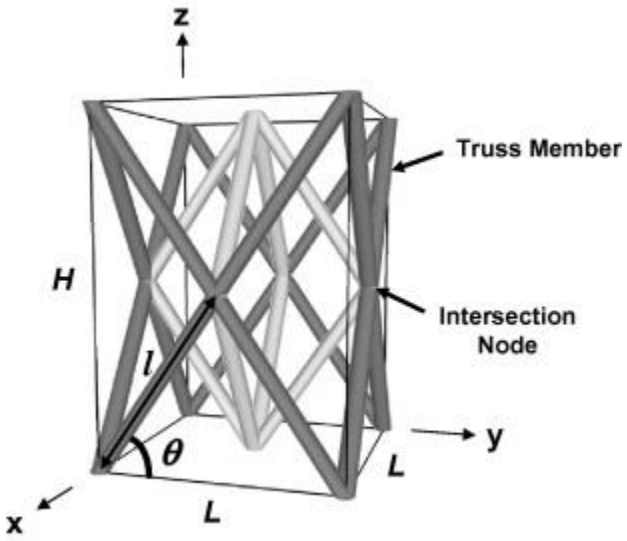

Figure 1: *Octrahedral-type unit cell of the polymer template used to fabricate the carbon micro-lattice structures [13].*

One polymer micro-lattice sample was fabricated for initial thermal gravimetric analysis (TGA) experiments and five additional polymer micro-lattice samples were fabricated for subsequent conversion to carbon. To increase the carbon yield of the samples prepared for pyrolysis, the polymer templates were submerged at room temperature (22 °C) in acrylonitrile (Aldrich) containing 1 wt.% photoinitiator (ESACURE KT046, Sartomer Co.). The mass increase of one sample was monitored every 30 min to determine a soak time sufficient for the acrylonitrile to completely penetrate the polymer micro-lattice template. A soak time of 3 h was sufficient for the system to reach equilibrium. After removing the micro-lattice samples from the acrylonitrile, pressurized nitrogen was used to remove all excess monomer that remained in the open porosity.

The five samples swollen with acrylonitrile were immediately placed in a nitrogen atmosphere and exposed to UV light (~7.5 mW cm^{-2}) to polymerize the acrylonitrile. A nitrogen atmosphere was required to remove oxygen, which acts as an inhibitor during the free-radical polymerization of

acrylonitrile. The samples were exposed for 1 min on each side to ensure complete polymerization over the entire sample.

The polymer micro-lattice fabrication capabilities limited the maximum size of each sample to approximately 34 × 34 × 9 mm thick. The outer edge of each sample (~5 mm wide border) contained an incomplete unit cell structure, which is a consequence of the intersecting self-propagating waveguide process. These edges were removed and used as the samples for subsequent thermal stabilization/pyrolysis experiments, density measurements, and characterization with X-ray diffraction. The internal portion of the samples impregnated with polyacrylonitrile (~24 × 24 × 9 mm thick) were used for preparation of the carbon micro-lattice compression samples.

2.2 Thermal stabilization

Thermal stabilization of polyacrylonitrile (PAN) is a technique used in the production of carbon fibers to increase the carbon yield during pyrolysis [17]. Stabilization of PAN is achieved through cyclization of the linear polymer chain, which occurs in an oxidative environment between 200 and 300 °C [17], [18] and [19]. Polymer micro-lattice samples impregnated with polyacrylonitrile (PAN) were thermally post-cured under different conditions to determine the ideal stabilization conditions. One sample each was post-cured at 130 °C under vacuum for 24 h and at 250 °C in air for 1, 12, 24, and 48 h. For comparison, a portion of the polymer micro-lattice sample without PAN was post-cured at 130 °C under vacuum for 24 h, and the remaining portion was post-cured at 250 °C for 24 h.

A thermogravametric analyzer (TGA Q500, TA Instruments) was used to determine the degradation temperature of the thiol-ene precursor polymer and the effect of thermal post-cure on the total mass loss of the micro-lattice material during pyrolysis. One micro-lattice sample was

heated in the TGA at 2 °C/min to determine the degradation temperature of the thiol-ene polymer in air. Samples impregnated with PAN were heated in the TGA at 2 °C/min to 1000 °C (the maximum temperature of the instrument) under an argon purge.

2.3 Carbon micro-lattice fabrication and characterization

The samples prepared for carbon characterization were post-cured at 250 °C for 24 h and subsequently heated at 2 °C/min to 1000 °C under an argon purge. The samples were held at 1000 °C for 1 h and then allowed to cool to room temperature under the argon purge in the furnace. A schematic representation of the processing steps for carbonization of the micro-lattice materials is shown in Fig. 2.

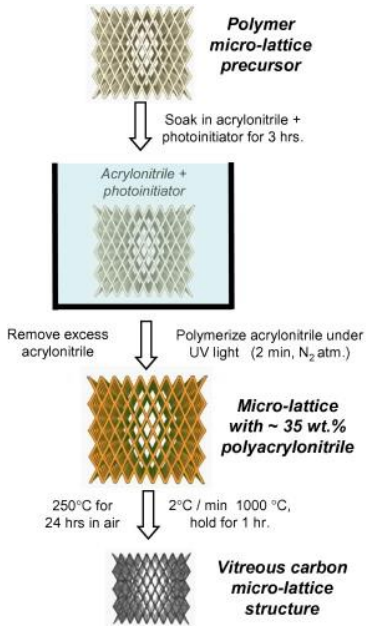

Figure 2: *The process for pyrolyzing the micro-lattice structures. The process involves impregnating and subsequently polymerizing acrylonitrile in the polymer precursor template. Polyacrylonitrile is added to increase the carbon yield of the resulting micro-lattice material after pyrolysis.*

Alan J. Jacobsen, Sky Mahoney, William B. Carter, Steven Nutt, Vitreous carbon micro-lattice structures, Carbon, Volume 49, Issue 3, March 2011, Pages 1025-1032, ISSN 0008-6223, http://dx.doi.org/10.1016/j.carbon.2010.10.059.

The density of the carbon that comprised the solid volume fraction of the micro-lattice structures was measured using a gas pycnometer with helium as the working fluid (MicroMeritics AccuPyc 1330). The average density was calculated from two different carbon samples, each measured five times with the gas pycnometer.

Powder X-ray diffraction was used to assess the crystallinity of the carbon material. Carbon micro-lattice samples were ground to a powder with a mortar and pestle and loaded into glass capillaries (1 mm outer diameter). The diffraction pattern was measured with Cu-K_α incident radiation (1.541874 Å) at 45 kV and a Ni filter was used to reduce the Cu-K_β radiation (Philips X'Pert MRD). The background from the glass capillary was measured separately and subtracted from the sample scans.

Diffraction patterns were also obtained on similarly prepared precursor polymers. The polymer samples included the cross-linked thiol-ene polymer, the thiol-ene polymer impregnated with PAN, and PAN that was photo-polymerized from acrylonitrile with 1 wt.% photo-initiator.

2.4 Mechanical characterization

The five thiol-ene/PAN polymer micro-lattice samples prepared for mechanical characterization were subjected to the same thermal post-cure and pyrolysis conditions described in Section 2.3. After pyrolysis, each sample measured approximately 16 × 16 × 6.6 mm. The volume change during pyrolysis caused slight curvature in the samples, so the top and bottom surfaces of each compression sample were ground flat. After grinding and polishing, each carbon micro-lattice sample was bonded between 0.25 mm thick steel face sheets with a rigid epoxy. A schematic of the carbon micro-lattice sample with face sheets is shown in Fig. 3.

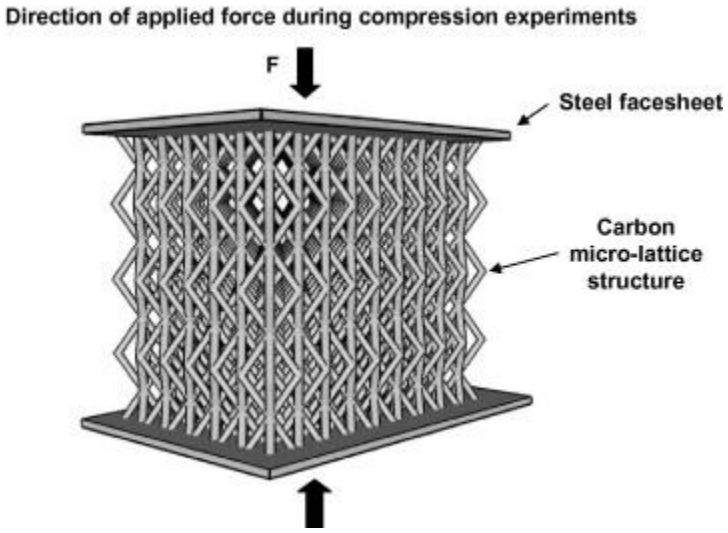

Figure 3: *A schematic of the carbon micro-lattice structures tested under compression.*

Quasi-static compression experiments were conducted on the five carbon micro-lattice samples. The samples were compressed to failure at a strain rate of 10^{-3} s^{-1}. The load was measured with a 15 kN load cell with an accuracy of ±1%. The displacement between the compression platens was measured with a laser extensometer. The accuracy of the compression stress calculated from the measured load and displacement was ±2%.

3. Results and discussion

3.1 Carbon micro-lattice fabrication

Fig. 4 includes images of the micro-lattice unit cell structure before and after impregnation and polymerization of the acrylonitrile. A stabilization temperature of 250 °C was selected for the thiol-ene/PAN polymer system to ensure sufficient stabilization of the PAN without significant degradation of the thiol-ene polymer phase.

Alan J. Jacobsen, Sky Mahoney, William B. Carter, Steven Nutt, Vitreous carbon micro-lattice structures, Carbon, Volume 49, Issue 3, March 2011, Pages 1025-1032, ISSN 0008-6223, http://dx.doi.org/10.1016/j.carbon.2010.10.059.

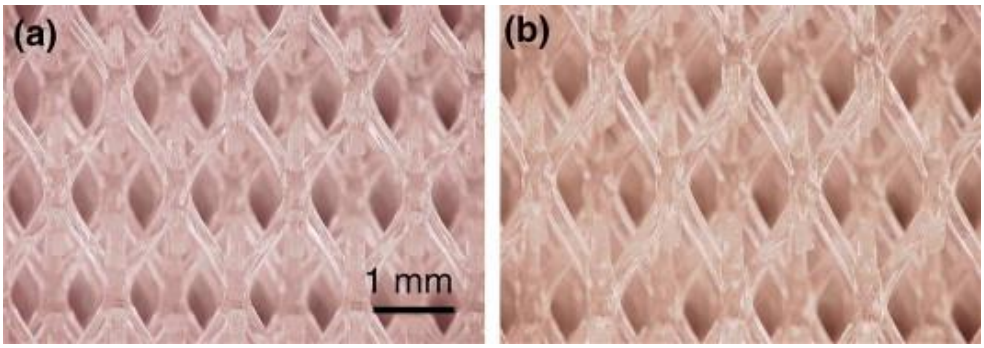

Figure 4: *(a) Polymer micro-lattice template, and (b) impregnated with ~35 wt.% polyacrylonitrile.*

The effects of different thermal post-cure conditions on the degradation of samples impregnated with PAN are included in Fig. 5. The residual weight at 1000 °C corresponds directly to the carbon yield of the sample. By thermally stabilizing the system at 250 °C in air for 1 h, the carbon yield was improved by 7% over a 24 h post-cure in vacuum. Increasing the thermal stabilization time to 24 h further increased the carbon yield by an additional 13%. However, thermal stabilization for 48 h at 250 °C in air caused a slight decrease in the carbon yield.

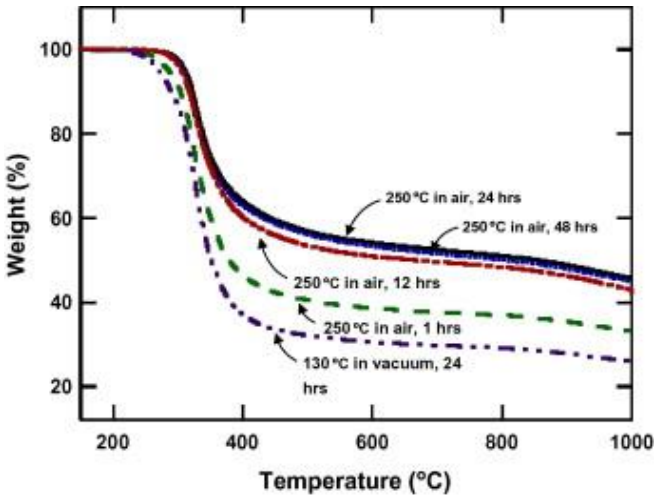

Figure 5: *The effect of different heat treatments on the mass loss of thiol-ene/PAN micro-lattice samples heated to 1000 °C (in argon). The results show a heat treatment at 250 °C in air for 24 h prior to pyrolysis maximizes the carbon yield of the micro-lattice samples.*

Alan J. Jacobsen, Sky Mahoney, William B. Carter, Steven Nutt, Vitreous carbon micro-lattice structures, Carbon, Volume 49, Issue 3, March 2011, Pages 1025-1032, ISSN 0008-6223, http://dx.doi.org/10.1016/j.carbon.2010.10.059.

The carbon yield of the micro-lattice samples with and without PAN are compared in Fig. 6. Without a thermal stabilization heat treatment prior to carbonization, the impregnation of 35 wt.% PAN increased the total carbon yield of the micro-lattice material from 18 to 26 wt.% at 1000 °C. However, a thermal stabilization heat treatment in air (24 h, 250 °C), in addition to the inclusion of PAN, increased the carbon yield to 46 wt.% at 1000 °C.

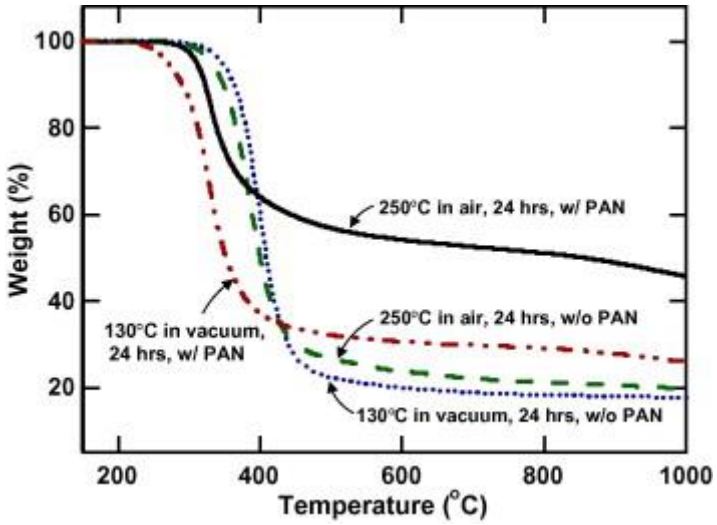

Figure 6: *A comparison of the mass loss (carbon yield) for polymer micro-lattice samples with and without the addition of polyacrylonitrile (PAN).*

Fig. 7a and b shows the micro-lattice unit cell structure after thermal stabilization heat treatment and after pyrolysis, respectively. The in-plane linear shrinkage of the micro-lattice structures was approximately 25%, which reduced the node-to-node spacing from approximately 1.3–1.0 mm.

Alan J. Jacobsen, Sky Mahoney, William B. Carter, Steven Nutt, Vitreous carbon micro-lattice structures, Carbon, Volume 49, Issue 3, March 2011, Pages 1025-1032, ISSN 0008-6223, http://dx.doi.org/10.1016/j.carbon.2010.10.059.

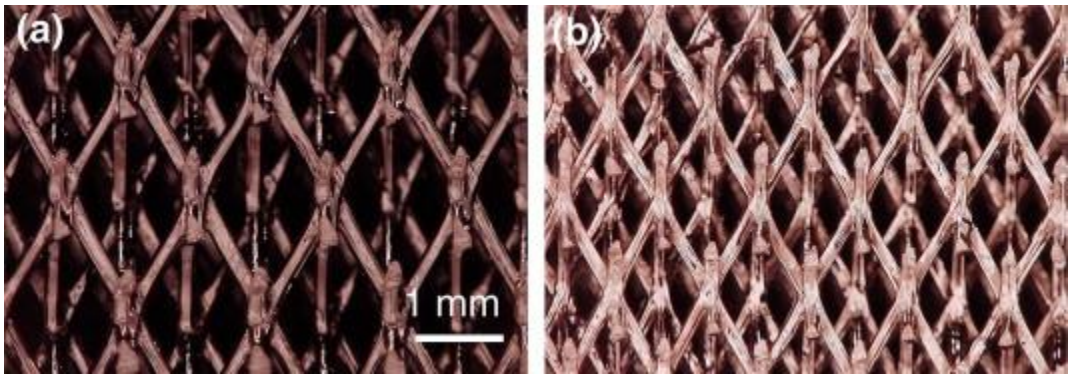

Figure 7: *(a) Polymer micro-lattice template impregnated with ~35 wt.% polyacrylonitrile and heated to 250 °C in air for 24 h, and (b) heated to 1000 °C in argon. The result is a vitreous carbon micro-lattice structure.*

For all samples, the TGA data is only shown for temperatures above 150 °C. Below approximately 100 °C, the micro-lattice samples post-cured at 250 °C in air exhibited up to 2% mass loss. An additional experiment was conducted to determine if this mass loss could be attributed to moisture that was absorbed by the samples after the thermal stabilization heat-treatment and before measurement in the TGA. A portion of the sample post-cured for 48 h was heated at 130 °C in vacuo (300 mtorr) for 4 days and split into two pieces, one of which was measured immediately. This sample exhibited no mass loss up to 150 °C. The remaining piece was left out in ambient lab conditions for 3 days, and subsequent measurement showed the low-temperature weight loss was present. To eliminate the contribution from moisture weight loss to the overall weight loss during pyrolysis, the measured weight loss of each sample was based on an initial mass at 150 °C. Further studies are required to characterize the conditions leading to ambient moisture absorption in the thermally stabilized polymer samples.

Alan J. Jacobsen, Sky Mahoney, William B. Carter, Steven Nutt, Vitreous carbon micro-lattice structures, Carbon, Volume 49, Issue 3, March 2011, Pages 1025-1032, ISSN 0008-6223, http://dx.doi.org/10.1016/j.carbon.2010.10.059.

3.2 Density and X-ray diffraction

One characteristic that differentiates vitreous carbon from diamond or pyrolytic graphite is its density, which is generally between 1.4 and 1.8 g cm^{-2}[8], [9] and [20]. The relatively low density of this form of carbon has been attributed to pores <0.3 nm distributed between the carbon crystallites [21]. The density of the solid carbon comprising the micro-lattice structures discussed in this study was 1.49 ± 0.004 g cm^{-3}. Previous work has shown that although vitreous carbon can exhibit nanoporosity, it is extremely impermeable to gases, and density measurements using helium are consistent with water displacement measurements [8] and [22].

Diffraction patterns for the precursor polymer materials and the carbon from a micro-lattice sample are shown in Fig. 8. The base thiol-ene polymer system showed a characteristic amorphous peak, whereas the semi-crystalline PAN polymer exhibited a sharp peak at $2\theta \approx 17.1°$. Note that the prominent peak associated with the crystalline phase of PAN polymer (~17°) was not present in the diffraction pattern of the thiol-ene/PAN polymer system. This indicates that when acrylonitrile was impregnated in the existing micro-lattice polymer and subsequently polymerized, the crystallinity of the PAN phase was suppressed.

Alan J. Jacobsen, Sky Mahoney, William B. Carter, Steven Nutt, Vitreous carbon micro-lattice structures, Carbon, Volume 49, Issue 3, March 2011, Pages 1025-1032, ISSN 0008-6223, http://dx.doi.org/10.1016/j.carbon.2010.10.059.

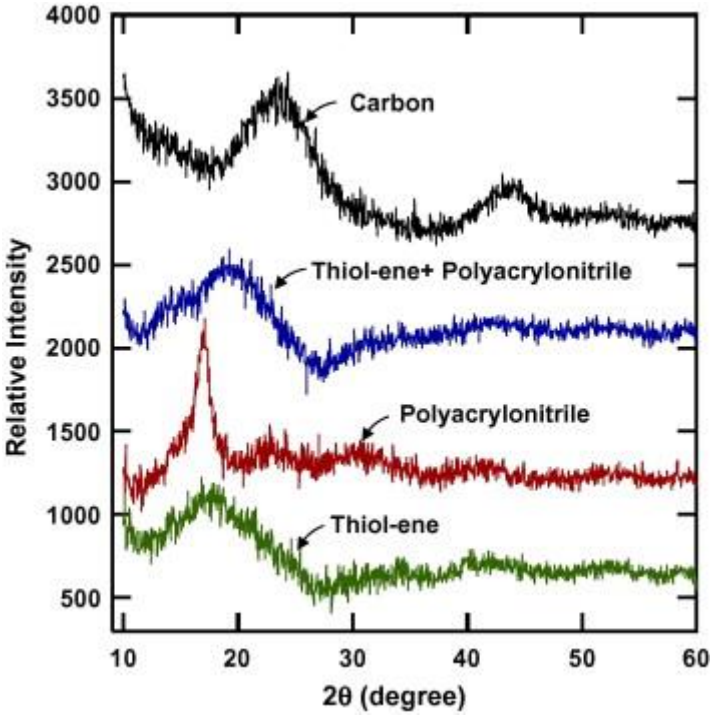

Figure 8: *X-ray diffraction patterns for the thiol-ene polymer used to fabricate the micro-lattice templates, polyacrylonitrile, thiol-ene impregnated with polyacrylonitrile, and carbon from a pyrolyzed micro-lattice sample.*

The measured diffraction pattern of the carbon material showed broad peaks at $2\theta \approx 23.5°$ and $2\theta \approx 43.5°$, corresponding to the (0 0 2) and (1 1 0) reflections from the carbon crystallites. The (0 0 2) peak corresponds to an approximate interlayer spacing of 3.8 Å (compared with 3.354 Å for ordered graphite), which is consistent with other XRD studies on vitreous carbon [8] and [22].

Alan J. Jacobsen, Sky Mahoney, William B. Carter, Steven Nutt, Vitreous carbon micro-lattice structures, Carbon, Volume 49, Issue 3, March 2011, Pages 1025-1032, ISSN 0008-6223, http://dx.doi.org/10.1016/j.carbon.2010.10.059.

3.3 Compression behaviour

3.3.1 Mechanical Analysis

The mechanical properties of an open-cellular material depend on the mechanical properties of the solid constituent material, the relative density of the cellular material, and the geometric configuration of the solid material, or cellular architecture. Extensive prior work has described the underlying mechanics of a cellular material, which links the cellular architecture to the bulk mechanical properties [23], [24] and [25]. Based on this prior work, Eqs. (1) and (2) describe the generalized relationships for the elastic modulus (E) and failure strength (σ) of a cellular material.

$$E = C_1 (E_s)(\rho/\rho_s)^{n_1} \quad (1)$$

$$\sigma = C_2 (\sigma_s)(\rho/\rho_s)^{n_2} \quad (2)$$

The terms E_s and σ_s are the elastic modulus and representative failure strength of the solid material, respectively. The term ρ/ρ_s is the relative density of the cellular material, which is defined as its density (ρ) divided by the density of the solid constituent material (ρ_s). The constants C_1 and C_2 are related to the geometric configuration of the cellular material with respect to the loading direction, and the constants n_1 and n_2 are a function of the deformation behavior of the cell struts (or lattice members) during mechanical loading.

According to the Gibson and Ashby model for brittle open-cellular foams, the cell struts exhibit bending-dominated deformation during elastic loading [23]. This type of deformation leads to a non-linear dependence of E and σ on the relative density ($n_1 = 2$ and $n_2 = 3/2$). Because of the complex nature of brittle failure, the proportionality constants, C_1 and C_2, are typically determined

empirically. In addition, the modulus of rupture (MOR, or flex strength) of the solid constituent material would best represent the failure strength σ_s in Eq. (2).

Conversely, an open-cellular lattice material can exhibit axial-dominated deformation (either tension or compression) of the lattice members if the cellular architecture is configured properly with respect to the direction of the mechanical load. Based on the assumption of axial-dominated deformation, Eq. (3) describes the compressive modulus (E) in the z-direction of the lattice unit cell shown in Fig. 1 [13] and [26]. A force balance in the z-direction can be used to derive Eq. (4), assuming failure of the brittle material occurs from a concentrated compressive force at the intersecting nodes.

$$E=(\sin^4\theta)(E_s)(\rho/\rho_s) \tag{3}$$

$$\sigma = \left(\frac{\sin\theta}{4}\right)(\sigma_s)(\rho/\rho_s) \tag{4}$$

As shown in Eqs. (3) and (4), both the compressive modulus and strength of the lattice material scale linearly with relative density (n_1 = 1 and n_2 = 1). Thus, at low relative densities, a lattice configuration can provide a substantial increase in the elastic modulus and strength of a cellular material compared to a random open-cell foam comprised of the same solid constituent material. This architectural benefit applies to both ductile and brittle constituent materials.

For a cellular material comprised of a ductile solid, the transition from bending-dominated to axial-dominated behavior will generally not change the representative solid material strength (σ_s) used in Eqs. (1) and (3). This is because for most ductile solids, the tensile and compressive strengths are similar. However, the modulus of rupture (MOR) can be significantly less than the compressive strength of brittle materials [9] and [20]. For example, the compression strength of vitreous carbon

reportedly can be more than 2× greater than the MOR. Thus, for brittle micro-lattice materials, the strength increase described by the mechanics of deformation is coupled with a substantial increase in the representative solid material strength.

3.3.2 Compression Results

Five carbon micro-lattice samples were tested under quasi-static compression. The average density of the samples was 0.19 ± 0.004 g cm^{-3}, and the corresponding average relative density was 12.8 ± 0.3%. Although all samples were fabricated under identical conditions and the relative density values were approximately equal, the compression behavior was markedly different, as shown in Fig. 9.

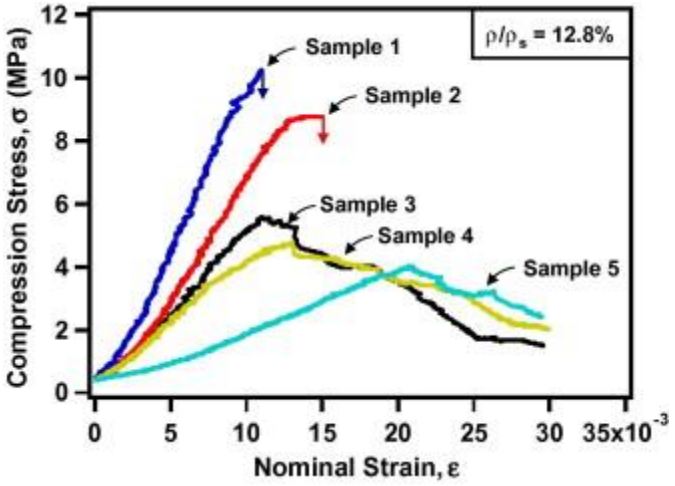

Figure 9: *Compression stress–strain results from five carbon micro-lattice samples with relative density = 12.8%. The difference in the stress–strain response was from non-uniform loading conditions during compression. Samples 1 and 2 failed catastrophically, whereas Samples 3–5 failed in localized regions.*

The elastic modulus and peak strength varied significantly between the five samples tested. The elastic modulus (*E*) of each sample was measured as the average slope of the stress–strain curve between 25% and 75% of the respective peak strength. For the five samples tested under

compression, the compressive modulus ranged from 0.2 GPa (Sample 5) to 1.1 GPa (Sample 1). The peak strength, taken as the stress at initial failure, ranged from 3.9 MPa for Sample 5 to 10.2 MPa for Sample 1.

The variation in the measured modulus between similar samples suggests non-uniform load distribution though the lattice members of each sample, which can be caused by samples with thickness variability and/or localized defects. For a flat sample with perfectly parallel compression surfaces, the entire cross-sectional area will contribute to the measured compressive load. However, for a carbon micro-lattice sample that has a small variation in thickness (parallelism), the regions of the sample that first come in contact with the compression platens will carry the bulk of the compressive load. The lattice members not in contact with the platens will only contribute to the load carrying capacity though load transfer at the nodes and bonded facesheets. In this case, the measured modulus will be less than the true modulus of the material because the effective cross-sectional area of each sample during compressive loading is less than the measured cross-sectional area used to calculate the stress. Samples with greater thickness variation will lead to larger stress concentrations in small portions of the sample, resulting in lower effective measured moduli. Likewise, a similar argument may be made for the variation in the measured peak strength between samples.

These results do not rule out the possibility of sample defects contributing to this variability as well. If localized defects prevent complete load transfer between the lattice members and/or nodes, this will also lead to non-uniform loading between the lattice members and result in a lower measured compressive modulus and peak strength. Further studies are necessary to understand the role defects on the compressive behavior of these carbon micro-lattice samples.

Alan J. Jacobsen, Sky Mahoney, William B. Carter, Steven Nutt, Vitreous carbon micro-lattice structures, Carbon, Volume 49, Issue 3, March 2011, Pages 1025-1032, ISSN 0008-6223, http://dx.doi.org/10.1016/j.carbon.2010.10.059.

The explanation for the variation in the measured compressive moduli and peak strengths offered above is further substantiated by observations of the failure of each sample. The two samples with the greatest peak strength values (Samples 1 and 2) exhibited full catastrophic failure from release of the stored elastic energy at initial fracture. In contrast, while the samples with lower measured elastic moduli and peak strengths (Samples 3–5) displayed similar initial catastrophic failure modes, the failure was localized to a portion of the overall sample as shown in Fig. 10.

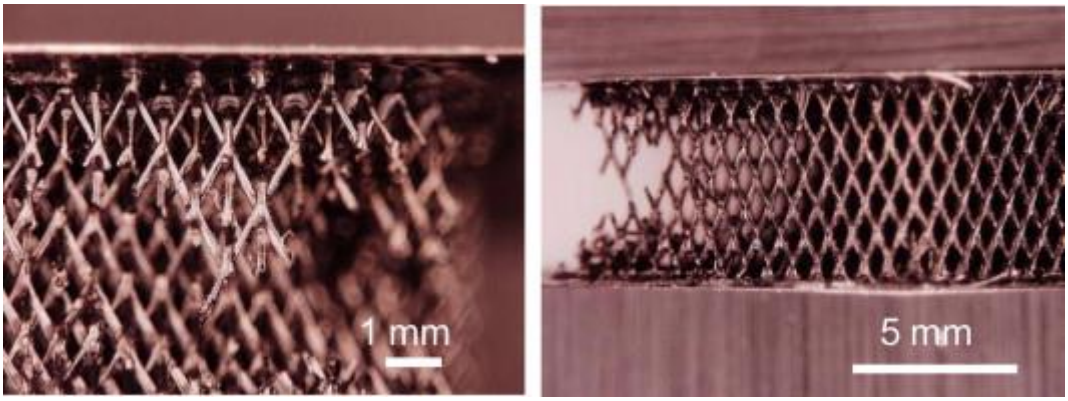

Figure 10: *Images of carbon micro-lattice sample (Sample 3) compressed to 0.3% strain. The sample failed in a localized region because of non-uniform load distribution during compression.*

Predicting the elastic modulus and peak strength of the micro-lattice structures requires accurate measurement of the bulk properties of vitreous carbon (E_s and σ_s). However, the methods described to form the vitreous carbon micro-lattice structures are difficult to translate to bulk samples; therefore, as an alternative evaluation of these experimental results, Eqs. (3) and (4) were used to estimate E_s and σ_s.

From Eq. (3), the measured values for Sample 1 (E = 1.1 GPa, ρ/ρ_s = 0.128, θ = 60°) gives E_s = 15 GPa. Published values for the elastic modulus of vitreous carbon vary between 20 and 35 GPa [8] and [9]. For comparison, when the lattice members exhibit bending-dominated deformation behavior (as is the case with RVC foams), Eq. (1) can be used to

estimate E_s (where C_1 = 1 and n_1 = 2 [23]). In this case, E_s is calculated to be 67 GPa, which is significantly greater than all reported elastic modulus values for vitreous carbon. Thus, the bending-dominated foam model is not an accurate description of the micro-lattice deformation behavior.

Although the estimated value for E_s of vitreous carbon obtained using Eq. (3) is below the range of values reported in the literature, these results indicate that the lattice member deformation is primarily axial-dominated before initial failure. The discrepancy between the value for E_s calculated here and values that appear in the literature is attributed to edge effects and non-ideal load distribution between the lattice members during compression.

In a similar manner, Eq. (4) can be used to estimate the failure strength of the solid vitreous carbon. Based on compression data for Sample 1, the estimated failure stress at the nodes was σ_s = 368 MPa. The compression strength reported in the literature for solid vitreous carbon ranges from 100 MPa to over 1 GPa [20] and [27] and the reported range for flexural strength is 60–280 MPa [9] and [20]. The large range of values reported for the compression and flexural strength of brittle vitreous carbon is because these properties are strongly dependent on processing parameters, precursor materials, and structural defects. Although the compression strength estimated here for the solid vitreous carbon is on the low end of the range reported in the literature, it is above the reported range for flexural strength. Considering that our analysis of the measured elastic modulus for Sample 1 indicates a non-ideal load distribution, this estimation for σ_s is consistent with our previous assertion that the carbon micro-lattices exhibited primarily axial-dominated deformation of the lattice members during compression.

The approach described here can be used to fabricate carbon micro-lattice materials with higher relative densities than RVC foams, and thus larger absolute peak strengths can be achieved. More

importantly, higher specific strengths are possible because of the micro-lattice architecture. For example, an RVC foam with a relative density of 4% tested with similar boundary conditions exhibited an average peak strength in compression of 0.85 MPa [28]. The specific strength (peak strength normalized by density) for Sample 1 was 53.7 kN mkg^{-1}, approximately 2.5× greater than the RVC foam.

Although carbon micro-lattice materials clearly show promise for improved mechanical performance in comparison to RVC foams, the mechanical properties are highly dependent on the uniform cellular architecture. The volumetric change during pyrolysis can lead to shape distortions within the sample, which makes it difficult to capture the exact intended cellular architecture and may lead to unintended stress concentrations during mechanical loading or residual stress induced defects.

4. Conclusions

A new approach to fabricate carbon open-cellular materials with a micro-lattice architecture is presented. The carbon micro-lattice samples were fabricated by pyrolyzing polymer templates that were formed from an interconnected pattern of photopolymer waveguides. Using a micro-lattice polymer structure as a precursor template, the remaining mass after pyrolysis increased from 19% to 46% with the inclusion of PAN. The resulting average density of the carbon micro-lattice samples was 0.19 g cm^{-3}. X-ray diffraction experiments and gas pycnometry measurements indicated the micro-lattice structures were comprised of vitreous carbon.

One advantage of a lattice configuration is the ability to uniformly distribute the load through the solid phase during compression. Compression tests conducted on carbon micro-lattice samples

Alan J. Jacobsen, Sky Mahoney, William B. Carter, Steven Nutt, Vitreous carbon micro-lattice structures, Carbon, Volume 49, Issue 3, March 2011, Pages 1025-1032, ISSN 0008-6223, http://dx.doi.org/10.1016/j.carbon.2010.10.059.

revealed large variability in the measured compressive modulus and peak strength, which has been attributed to non-uniform loading and potential defects within the samples. Of the samples tested, the largest measured peak strength was 10.2 MPa (53.7 kN mkg^{-1} specific strength), significantly greater than the specific strength of available RVC foams (~21.3 kN mkg^{-1}).

The described process produced micro-lattice structures of vitreous carbon, and we assumed there was no (0 0 2) orientation along the concentric axes of the lattice members. However, reducing the unit cell feature size in combination with applied tensile stresses during heat treatment may provide a path to achieve such as material. If such a structure can be achieved, one could realize the mechanical benefits that result from alignment of C–C bonds within the (0 0 2) planes, as in traditional PAN-based carbon fibers. In combination with the lattice architecture, these properties could translate to a three-dimensional, bulk open-cellular material with further improved specific properties.

The approach described here to fabricate carbon micro-lattice materials can be used to produce a wide range of relative densities and unit cell architectures. This design flexibility enables optimization for multifunctional applications that require the material to carry mechanical loads while simultaneously transporting fluid within the open architecture. Such functionality is highly desirable for heat transfer media or electrodes for electrochemical devices.

References:

1. Gaefke CB, Botelho EC, Ferreira NG, Rezende MC. Effect of furfuryl alcohol addition on the cure of furfuryl alcohol resin used in the glassy carbon manufacture. J Appl Polym Sci 2007;106:2274–81.
2. Czerwinski A, Rogulski Z, Obrebowski S, Siwek H, Paleska I, et al. RVC as new carbon material for batteries. J Appl Electrochem 2009;39(5):559–67.
3. Wang J. Reticulated vitreous carbon–a new versatile electrode material. Electrochim Acta 1981;26(12):1721–6.

Alan J. Jacobsen, Sky Mahoney, William B. Carter, Steven Nutt, Vitreous carbon micro-lattice structures, Carbon, Volume 49, Issue 3, March 2011, Pages 1025-1032, ISSN 0008-6223, http://dx.doi.org/10.1016/j.carbon.2010.10.059.

4. Friedrich JM, Ponce-De-Leon C, Reade GW, Walsh FC. Reticulated vitreous carbon as an electrode material. J Electroanal Chem 2004;561(1–2):203–17.
5. Pandolfo AG, Hollenkamp AF. Carbon properties and their role in supercapacitors. J Power Sources 2006;157(1):11–27.
6. Strohl AN, Curran DJ. Reticulated vitreous carbon flowthrough electrodes. Anal Chem 1979;51(3):353–7.
7. Gallego NC, Klett JW. Carbon foams for thermal management. Carbon 2003;41(7):1461–6.
8. Cowlard FC, Lewis JC. Vitreous carbon–a new form of carbon. J Mater Sci 1970;2(6):507–12.
9. Pierson HO. Handbook of carbon, graphite, diamond, and fullerenes; properties, processing, and applications. Park Ridge, NJ: Noyes Publications; 1993.
10. Tondi G, Fierro V, Pizzi A, Celzard A. Tannin-based carbon foams. Carbon 2009;47(6):1480–92.
11. Pekala RW, Hopper RW. Low-density microcellular carbon foams. J Mater Sci 1987;22(5):1840–4.
12. Jacobsen AJ, Barvosa-Carter W, Nutt S. Micro-scale truss structures formed from self-propagating photopolymer waveguides. Adv Mater 2007;19(22):3892–6.
13. Jacobsen AJ, Barvosa-Carter W, Nutt S. Compression behavior of micro-scale truss structures formed from self-propagating polymer waveguides. Acta Mater 2007;55(20):6724–33.
14. Jacobsen AJ, Barvosa-Carter W, Nutt S. Micro-scale truss structures with three-fold and six-fold symmetry formed from self-propagating polymer waveguides. Acta Mater 2008;56(11):2540–8.
15. Fried JR. Polymer science and technology. 2nd ed. Prentice Hall PTR; 2003.
16. Giunta PR, Bossio RE, Stiegman AE, Marshall AG. Photochemically generated polyacrylonitrile-silica nanocomposites: optimized fabrication and characterization. Chem Mater 2003;15(6):1289–95.
17. Dalton S, Heatley F, Budd PM. Thermal stabilization of polyacrylonitrile fibres. Polymer 1999;40(20):5531–43.
18. Aubert JH, Sylwester AP. Morphological characterization of microcellular carbon foams. J Mater Sci 1991;26(21):5741–52.
19. Bajaj P, Sreekumar TV, Sen K. Thermal behaviour of acrylonitrile copolymers having methacrylic and itaconic acid comonomers. Polymer 2001;42(4):1707–18.
20. Jenkins GMK. K. Polymeric carbons: carbon fiber, glass, and char. Cambridge, UK: Cambridge University Press; 1976.
21. Manocha LM. Carbon, ordered to disordered materials. Mater Sci Forum 1996;223–224:117–26.
22. Harikrishnan G, Patro TU, Khakhar DV. Reticulated vitreous carbon from polyurethane foam-clay composites. Carbon 2007;45(3):531–5.
23. Gibson LJA MF. Cellular solids: structure and properties. 2nd ed. Cambridge, UK: Cambridge University Press; 1997.
24. Ashby MF. The properties of foams and lattices. Philos Trans R Soc A-Math Phys Eng Sci 2006;364(1838):15–30.
25. Deshpande VS, Ashby MF, Fleck NA. Foam topology bending versus stretching dominated architectures. Acta Mater 2001;49(6):1035–40.
26. Deshpande VS, Fleck NA. Collapse of truss core sandwich beams in 3-point bending. Int J Solids Struct 2001;38(36– 37):6275–305.
27. Brezny R, Green DJ. The effect of cell-size on the mechanicalbehavior of cellular materials. Acta Metall Mater 1990;38(12):2517–26.
28. Brezny R, Green DJ. Uniaxial strength behavior of brittle cellular materials. J Am Ceram Soc 1993;76(9):2185–92.

Alan J. Jacobsen, Sky Mahoney, William B. Carter, Steven Nutt, Vitreous carbon micro-lattice structures, Carbon, Volume 49, Issue 3, March 2011, Pages 1025-1032, ISSN 0008-6223, http://dx.doi.org/10.1016/j.carbon.2010.10.059.